Sub-keV energy model for nuclear recoil depositions in liquid noble elements for CEνNS and Dark matter direct searches. Results and perspectives of the Skipper-CCD at ICN detector laboratory

Depto. Altas Energías

Dr. Youssef Sarkis & Dr. Juan Carlos D'Olivo

Instituto de Ciencias Nucleares, UNAM

Seminario de Física de Altas Energías. ICN

5 de noviembre de 2025

Contents

Motivation

COHERENT NEUTRINO-NUCLEUS SCATTERING (CEνNS)

- Occurrence of neutral-current neutrino interactions in the Standard Model.
- The existence of elastic neutrino-nucleus scattering proposed for the first time in 1974 (no energy threshold) [1] .

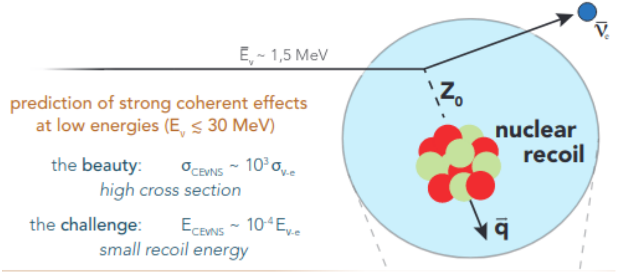

[1] **Predicted in 1975 by D.Z. Freedman in 1973, V.B. Kopeliovich and L.L. Frankfurt, JETP Lett. 19 4 236 (1974)**. First detected by the COHERENT collaboration in 2017 with CsI crystals (2021 and 2024 in LAr and Ge).

Coherent Elastic Neutrino–Nucleus Scattering (CEνNS)

- Large cross section compared to inverse beta decay process.
- Purely neutral-current process mediated by Z boson exchange.
- Coherence condition: $qR_A \lesssim 1$, typically for $E_\nu \lesssim 50$ MeV.

Standard Model contribution:

$$\frac{d\sigma}{dT} = \frac{G_F^2 m_A}{4\pi}\left(1 - \frac{m_A T}{2E_\nu^2}\right) Q_w^2 \left|F_w(q^2)\right|^2$$

- Provides access to the weak nuclear charge:

$$Q_w = N - (1 - 4\sin^2\theta_W)Z$$

- m_A: nuclear mass, T: recoil energy, E_ν: neutrino energy.
- $F_w(q^2)$: weak form factor (depends on neutron density distribution).
- Coherent enhancement $\propto N^2$ for spin-0 nuclei.

Spallation Source

- Pion decay at rest source.
- Well-known fluxes.
- Neutrino energies above 20 MeV.

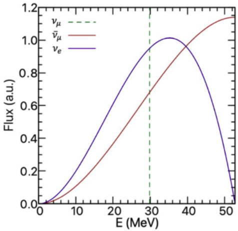

Reactor Source

- Neutrinos from nuclear decays.
- Huber-Muller model for $E > 1{,}8$ MeV.
- Uncertainty in flux normalization $\approx 3\,\%$.
- Neutrino energies below 10 MeV.

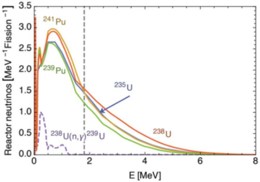

Solar Neutrino Source

- Neutrinos from reactions within the sun.
- Currently sensitive to ^{8}B flux.
- Neutrino energies below 1 MeV.

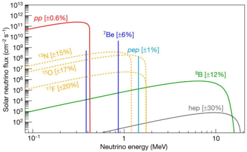

Light Mediators Z'

- ν interact via Z-boson exchange, with a heavy mass $M_Z \approx 91$ GeV.
- Z' modifies neutrino–nucleus-electron scattering cross sections [2].
- Could explain LSND-MiniBooNE and Gallium Anomaly.
- Dark neutrino portal.
- $U'(1)$ gauge symmetry

$$\left.\frac{\mathrm{d}\sigma_{\nu\mathcal{N}}}{\mathrm{d}T_{\mathcal{N}}}\right|^{S}_{\mathrm{CE}\nu\mathrm{NS}} = \frac{m_{\mathcal{N}}\mathcal{Q}_S^2}{4\pi\left(m_S^2 + 2m_{\mathcal{N}}T_{\mathcal{N}}\right)^2} F_W^2\left(|\mathbf{q}|^2\right)\frac{m_{\mathcal{N}}T_{\mathcal{N}}}{E_\nu^2}$$

$$\left.\frac{\mathrm{d}\sigma_{\nu\mathcal{N}}}{\mathrm{d}T_{\mathcal{N}}}\right|^{V}_{\mathrm{CE}\nu\mathrm{NS}} = \left[1 + \kappa\frac{Q_{\mathrm{w}}}{\sqrt{2}G_F Q_V^{\mathrm{SM}}\left(m_V^2 + 2m_{\mathcal{N}}T_{\mathcal{N}}\right)}\right]^2 \left.\frac{\mathrm{d}\sigma_{\nu\mathcal{N}}}{\mathrm{d}T_{\mathcal{N}}}\right|^{\mathrm{SM}}_{\mathrm{CE}\nu\mathrm{NS}},$$

Observables:

Shift in CEνNS recoil spectrum shape.

[2] Aguilar-Arevalo, Alexis et al,JHEP04(2020)054

Non-Standard Interactions (NSI)

$$\mathcal{L}_{\text{NSI}} = -2\sqrt{2}G_F \sum_{q,\alpha,\beta} \epsilon_{\alpha\beta}^{qP} \left(\bar{\nu}_\alpha \gamma_\mu P_L \nu_\beta\right) \left(\bar{q}\gamma^\mu P q\right)$$

$$\begin{aligned}\left(Q_V^{\mathrm{NSI}}\right)^2 =& \left[Z\left(g_V^p + 2\varepsilon_{\ell\ell}^{uV} + \varepsilon_{\ell\ell}^{dV}\right) + N\left(g_V^n + \varepsilon_{\ell\ell}^{uV} + 2\varepsilon_{\ell\ell}^{dV}\right)\right]^2 \\ &+ \sum_{\ell<\ell''} \left|Z\left(2\varepsilon_{\ell\ell'}^{uV} + \varepsilon_{\ell\ell'}^{dV}\right) + N\left(\varepsilon_{\ell\ell'}^{uV} + 2\varepsilon_{\ell\ell'}^{dV}\right)\right|^* .\end{aligned}$$

- $\epsilon_{\alpha\beta}^{qP}$ quantify deviations from SM couplings[3].
- Modify the effective weak charge of the neutrino in scattering or matter interactions.
- Flavor-conserving: modifies normalization of cross section.
- Flavor-changing: induces $\nu_\alpha \to \nu_\beta$ modify oscillation probabilities in matter.
- Low-energy manifestation of high-scale BSM physics.

Observables:

Shift in CEνNS recoil spectrum shape.

[3] Barranco, Miranda, and Rashba JHEP 12 (2005) 021

Neutrino Magnetic Moment

- Extension to SM with massive neutrinos.
- A neutrino coupling to the photon can be induced at a loop level.

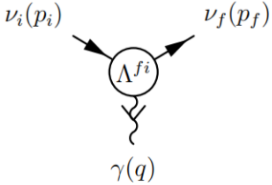

- Respect Lorentz and gauge symmetries
- Single parameter suitable for phenomenological analysis.

$$\left.\frac{\mathrm{d}\sigma_{\nu\mathcal{N}}}{\mathrm{d}T_N}\right|_{\mathrm{CE}\nu\mathrm{NS}}^{\mathrm{MM}} = \frac{\pi\alpha_{\mathrm{EM}}^2}{m_e^2}\left(\frac{1}{T_N} - \frac{1}{E_\nu}\right) Z^2 F_W^2\left(|\mathbf{q}|^2\right)\left|\frac{\mu_{\nu_\ell}^{\mathrm{eff}}}{\mu_{\mathrm{B}}}\right|^2$$

- Relevant at low recoil energies

Other Extensions

- Generalized Neutrino Interactions (GNI):
  - Extension to SM including all Lorentz invariant interactions.
  - Only sensitive to scalar and vector interactions
- Sterile dipole portal:
  - Sterile neutrino of mass of mass m_4.
  - Electromagnetic coupling at loop level.
- Sterile fermion:
  - Sterile dark fermion in the MeV range.
  - Interaction mediated by a scalar or vector.
- Neutrino background for dark matter searches:
  - CEνNs can give us information for directional searches.
  - Extent direct dark matter searches.

Theoretical Challenges

- Uncertainties in weak form factors and neutron skin ($R_n - R_p$).
- Nuclear many-body corrections (two-body currents).
- Spin-dependent (axial) contributions not fully coherent.
- Matching between EFT Wilson coefficients and hadron matrix elements.

Instituto de Ciencias Nucleares UNAM

Experimental Challenges

- **Low recoil energies:** Thresholds < 10 keV needed for full CEνNS signal.
- **Detector systematics:**
  - Nuclear ionization Efficiency (quenching factor).
  - Energy resolution, nuclear and electronic Fano factors.
  - Timing and mass scaling.
- **Background control:** reactor and spallation sources have complex spectra.
- **Degeneracies:** between NSI and nuclear-structure uncertainties [4].

Aim

A precision gateway to MeV-scale new physics.

Nuclear ionization efficiency comprehension remain as one of the main challenges!

[4] D. Aristizabal Sierra et al,JHEP 1906:141 (2019)

Ionization Efficiency Theory

Definition

- In a pure media, e.g. Si, Ge or liquid noble.
- Non ionizing particle hits a nuclei with energy E_R.
- Produces a cascade of ions until the energy is not sufficient to overcome binding.
- The energy goes into:
  - Electronic energy.
  - Atomic motion.
- We defined the **Nuclear Ionization Efficiency:** $\boxed{f_n(E_R) = \frac{E_{ee}}{E_R}}$
- It should have a low energy E_U threshold: $f_n(2E_U) = 0$.
- Depends mainly of the electronic S_e and nuclear S_n stopping power.
- High energies $S_e \gg S_n$, so $f_n \to 1$.

Measurements are challenging! (Si and Ge quenching factor measurements)

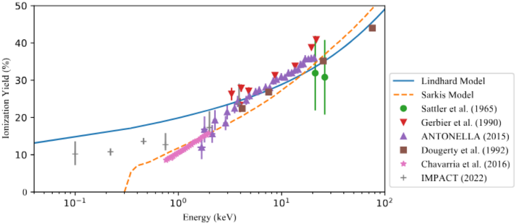

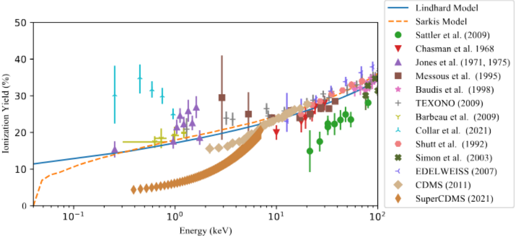

Especially at low energies.

Basic Integral Equation and Approximations

$\boxed{\text{Total Energy (electronic + nuclear): } \varepsilon_R = \bar{\eta}(\varepsilon) + \bar{\nu}(\varepsilon)\text{, in adimensional units } \varepsilon = (\frac{11{,}5}{Z^{7/3}\mathrm{keV}})E}$

$$\underbrace{\int d\sigma_{n,e}}_{\text{total cross section}} \left[\underbrace{\bar{\nu}\left(E - T_n - \sum_i T_{ei}\right)}_{A} + \underbrace{\bar{\nu}\,(T_n - U)}_{B} + \underbrace{\bar{\nu}(E)}_{C} + \underbrace{\sum_i \bar{\nu}_e\,(T_{ei} - U_{ei})}_{D} \right] = 0 \qquad (1)$$

Lindhard's (five) approximations[a]

- I Neglect contribution to atomic motion coming from electrons.
- II **Neglect the binding energy, $U = 0$.**
- III Energy transferred to electrons is small compared to that transferred to recoil ions.
- IV Effects of electronic and atomic collisions can be treated separately.
- V T_n is also small compared to the energy E.

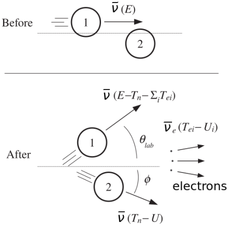

[a] (T_n : Nuclear kinetic energy and T_{ei} electron kinetic energy.)

Lindhard Simplified Equation

Using the five approximations Lindhard deduced an integral simplified equation,

$$\underbrace{\left(k\varepsilon^{1/2}\right)}_{S_e}\bar{\nu}'(\varepsilon) = \int_0^{\varepsilon^2} \underbrace{dt\frac{f\left(t^{1/2}\right)}{2t^{3/2}}}_{d\sigma_n}\left[\bar{\nu}(\varepsilon - t/\varepsilon) + \bar{\nu}(t/\varepsilon) - \bar{\nu}(\varepsilon)\right], \qquad (2)$$

L.H.S R.H.S

- Eq. (2) valid only at high energies.
- Elec. stop. valid for $E > 10\ keV$.
- Lindhard deduce a parametrization valid at high energies (U=0),

$\rightarrow$

$$\bar{\nu}_L(\varepsilon) = \frac{\varepsilon}{1 + kg(\varepsilon)},\ g(\varepsilon) = 3\varepsilon^{0,15} + 0,7\varepsilon^{0,6} + \varepsilon.$$

- **But fails below 4 keV in Si.**

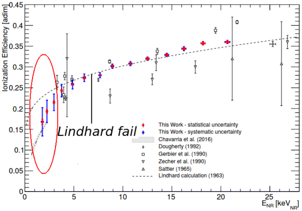

PRD Chavarria et al., 94, 082007(2016)

Instituto de Ciencias Nucleares UNAM

Simplified equation with binding energy

- We deduce a second-order integro-differential equation for atomic motion.[5].

$$-\frac{1}{2}\varepsilon S_e(\varepsilon)\left(1+\frac{W(\varepsilon)}{S_e(\varepsilon)\varepsilon}\right)\bar{\nu}''(\varepsilon)+S_e(\varepsilon)\bar{\nu}'(\varepsilon)=\int_{\varepsilon u}^{\varepsilon^2} dt\,\frac{f\left(t^{1/2}\right)}{2t^{3/2}}\left[\bar{\nu}(\varepsilon-t/\varepsilon)+\bar{\nu}(t/\varepsilon-u)-\bar{\nu}(\varepsilon)\right], \tag{3}$$

This work have been used for **Skipper CCD's: (DAMIC) PRD 109 (2024) 6, 062007 and (CONNIE) e-Print: 2403.15976.**

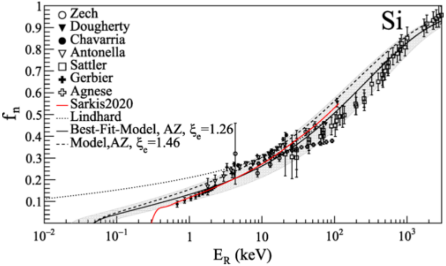

- Electronic stopping S_e with Coulomb repulsion effects (Ziegler potential).
- Bohr electron stripping for ions.
- Threshold limited by Frenkel pair energy.
- Electronic straggling effect $W(\varepsilon)$.
- Scaling factor ξ_e from Pauli principle, instead of Lindhard semi-empirical factor $\xi_e \approx Z^{1/6}$.

[5] Sarkis, Y. and Aguilar-Arevalo, A. and D'Olivo, J. C, PRA.107.062811

Improvements for S_e

- We use Tilinin model to compute the electronic stopping power.

$$S_e = (\xi_e) N m v \int_R^{\infty} v_F \sigma_{\mathbf{tr}}(v_F) N_e dV, \quad E = \phi_Z(R_0)$$

- We use data for $e-$ atom Momentum Transfer Cross Section
- We implement a hard-Sphere energy dependent potential model.
- Valid for lower energies compare to Tilinin semi-classical approach.

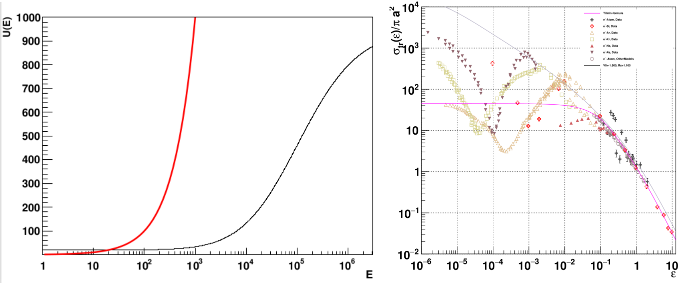

Figura: (left) Energy dependent binding energy, (right) σ_{tr} for Atom-e.

Physical interpretation of Scaling length ξ_e

- The scaling length determine the energy fraction of free electrons [6].

$$\xi_e^{2/3} \equiv \frac{5}{3}\frac{4\pi\int_{k_F-\Delta}^{k_F} E(k)k^2dk}{4\pi E(k_F)\int_{k_F-\Delta}^{k_F} k^2dk},\ E(k) = \frac{(\hbar k)^2}{2m} \text{ and } E_F = U_{TF}/\xi_e^{2/3}.$$

- For $\Delta \to 0$ then $\xi_e \to (5/3)^{3/2} \approx 2{,}15, \quad \Delta \to\ k_F$ then $\xi_e \to 1$.
- No electron collisions and radial collisions.
- Improves radial Thomas-Fermi model.
- E_Δ, energy available for free electrons.
- Cascade of ions produce a plasma with E_Δ electron energy.
- For Si, $\xi_e = 1{,}26$ and LXe $\xi_e = 1{,}19$, this gives $E_\Delta = 88$ eV and $E_\Delta = 850$ eV.

[6] In the context of Thomas-Fermi model.

Total Quanta for Liquid Noble Detectors

Liquid Noble TPC

- Dual-phase Time Projection Chamber (TPC).
- Light n_γ and Charge n_e detection combined to obtain Particle track.
- Primary scintillation (S1) from interaction in liquid.
- Secondary light signal (S2) from ionization electrons accelerated in gas chamber.
- Discrimination of nuclear recoil (NR) and electron recoil (ER) signals.
- Total quanta:

$$E_{\mathrm{ee}} = W\left(\frac{S1}{g_1} + \frac{S2}{g_2}\right), \rightarrow$$

$$E_R f_n(E_R) = W\,\underbrace{(n_\gamma + n_e)}_{\textbf{Total Quanta}},$$

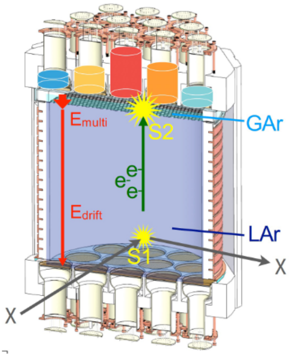

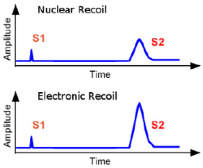

Thomas-Imel box Model

- Diffusion equation for ions-electrons (N_- N_+) Jaffe model, [7].

$$\frac{\partial N_+}{\partial t} = -\alpha N_- N_+, \qquad \frac{\partial N_-}{\partial t} = \mu_e F \frac{\partial N_-}{\partial z} - \alpha N_+ N_-. \qquad (4)$$

- Where α is the recombination factor, μ_e electron mobility and F the TPC electric field.
- Each excited or ionized atom leads to one photon or electron.
- $\Rightarrow N_i + N_{ex} = n_\gamma + n_e$,
- $n_e = (1 - r)N_i$ and $n_\gamma = N_{ex} + rN_i$.
- Hence, the fraction of ionizations predicted is

$$\frac{n_e}{N_i} = \frac{1}{\xi}\ln(1+\xi), \quad 1 - r = \frac{1}{\xi}\ln\left(1+\xi\right), \quad \xi = \frac{N_i \alpha}{4a^2 \mu_e F}.$$

$$N_i = \frac{E_R \mathbf{f_n}}{W(1+\beta)}, \quad \text{Where } \beta = N_{ex}/N_i \text{ and } f_n = \frac{E_{ee}}{E_R}.$$

- This recombination model depends on **four parameters for each noble liquid.**

[7] Ann.Phys.IV, V42, pp.303 − 344, (1913). PRA 36, 614 (1987)

- The model usually needs more than 10 parameters to work.
- Difficult to implement and could produce degeneracies.

Parameter	NEST v2	Run1 subleading
α	$11.0^{+2.0}_{-0.5}$	$12.0^{+1.7}_{-1.1}$
β	$1.10^{+0.05}_{-0.05}$	$1.10^{+0.06}_{-0.04}$
γ	$0.0480^{+0.0021}_{-0.0021}$	$0.0482^{+0.0014}_{-0.0018}$
ϵ	$12.6^{+3.4}_{-2.9}$	$14.7^{+3.1}_{-3.0}$
ζ	$0.3^{+0.1}_{-0.1}$	$0.3^{+0.2}_{-0.1}$
η	2^{+1}_{-1}	2^{+2}_{-1}
θ	$0.30^{+0.05}_{-0.05}$	$0.30^{+0.06}_{-0.06}$
ι	$2.0^{+0.5}_{-0.5}$	$2.2^{+0.7}_{-0.7}$
F_{ex}	0.4	$0.5^{+0.4}_{-0.4}$
F_i	0.4	$0.4^{+0.4}_{-0.3}$
ξ	0.59	$0.53^{+0.28}_{-0.36}$
ω	0.19	$0.21^{+0.52}_{-0.18}$

$$Q_y^{ER} = \left(\boxed{\frac{1}{\gamma}} + \boxed{p_0\,(E_{er}/\mathrm{keV}_{er})^{p_1}}\right)\boxed{\frac{\ln(1+\gamma\,\rho\,E_{er})}{E_{er}}}$$

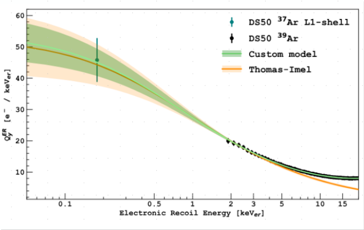

- Table from PandaX neutron studies and David deFranco at LIDINe2025.
- In this form the model most be modified.

- For electron calibration $f_n \equiv 1$ then, $1/W = (n_\gamma + n_e)/E_{ee}$.
- Electron-Atom interaction only, then $N_{ex}/N_i \approx 0{,}1$ constant.

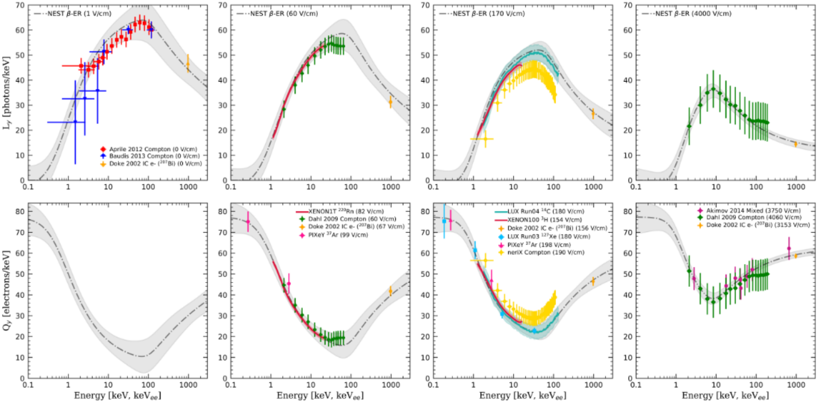

- For nuclear recoils $f_n < 1$.
- Atom-Atom interaction, then $N_{ex}/N_i \approx 1$.

LXe data

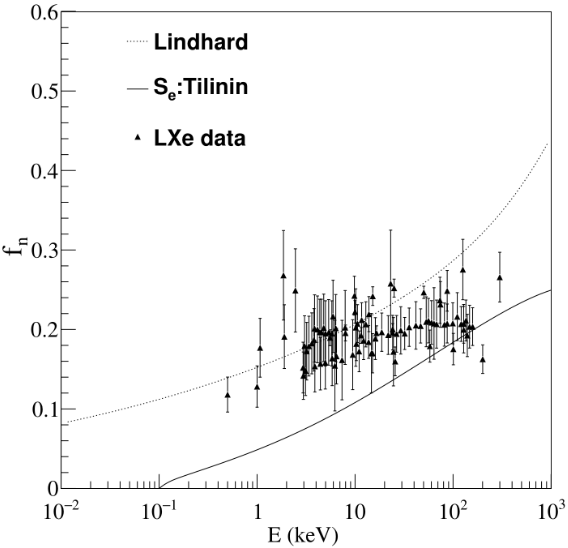

0.6
0.5
0.4
0.3
0.2
0.1
0
f_n
Lindhard
S_e:Tilinin
LXe data
10^{-2}
10^{-1}
1
10
10^2
10^3
E (keV)

Bates-Griffing Process (BG)

- For two atoms collision, we can take the valence electrons wave function: $\psi(x_1', x_2')_{\pm} = (\psi_1(x_1')\psi_2(x_2') \pm \psi_1(x_2')\psi_2(x_1'))/\sqrt{2}$.
- This leads to exchange electron non classical potential.
- $\psi(x_1', x_2')_{-}$ (triplet): **Passive electrons**, remains in its ground state (or excited) during the interaction with the target electron.

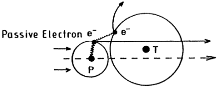

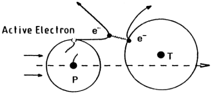

- $\psi(x_1', x_2')_{+}$ (singlet): **Active electrons,** the projectile electron is removed from its ground state.
- This define the average ionization energy to remove an electron for two atoms collision: $W_i = W(1 + N_{ex}/N_i)$.

- Effective Ziegler e-Atom potential and e-e Coulomb potential.
- Both potentials most overcome the electron binding of the outer orbital.

$$\frac{U_e}{2} = \frac{e\phi_Z^e(y', \xi_e, N)}{2} + \frac{e^2}{bx'}.$$

- We get x distance by solving for $y = \sqrt{x_0^2 + x^2}$.
- From this we compute the average energy for Atom-Atom ionization,

$$\frac{W_i(E, \xi_e)}{2} = \frac{e\phi_Z(x, \xi_e)}{2},$$

- Assuming that excitons and ions recombine,

$$\frac{N_{ex}}{N_i}(E, \xi_e) = \left(\frac{W_i(E, \xi_e)}{W} - 1 \right),$$

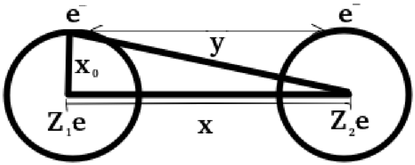

- Bohr stripping criteria to compute effective number of electrons at high energies.

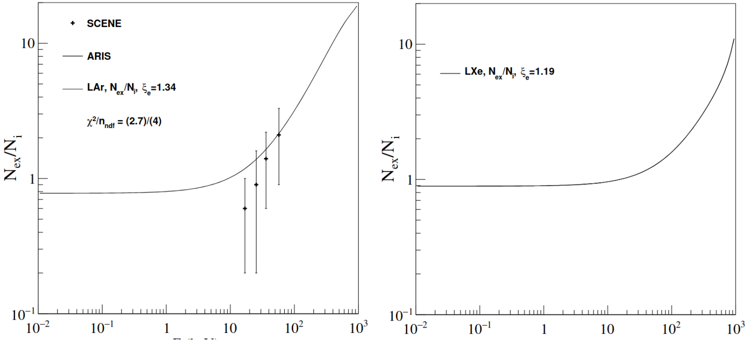

- Exciton to ion ratio for LAr and LXe.
- This effect correct Charge yield at high energies!.

Biexcitonic Process

Model with Birks law

$$f_l = \frac{1}{1 + k_{Birks} S_e}$$

- The observable light is reduced.
- $(\frac{E_R}{W}) f_n^M = (n_e + n_\gamma) \leq (n_e + n_\gamma / f_l)$.

$$f_n^M = f_n f_l + (1 - f_l)(n_e / E_R) W,$$

- The Birks parameter have to be proportional $S_e(\varepsilon_0, \xi_e)^{-1}$
- $\xi_e k_B = \frac{1}{4} \left(\frac{7{,}52}{\varepsilon_0^{1/2}} \right) \left(\frac{A}{Z} \right)^{1/2}$,
- $k_{Birks} = 4{,}2$ in LAr and $k_{Birks} = 5{,}3$ in LXe .
- $\varepsilon_0 = (u_{TF} - \varepsilon_\Delta) Z$.

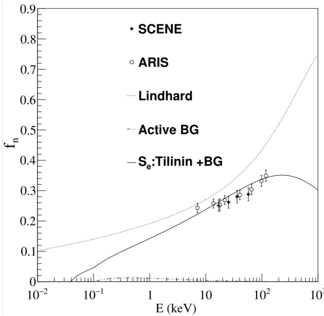

LXe data

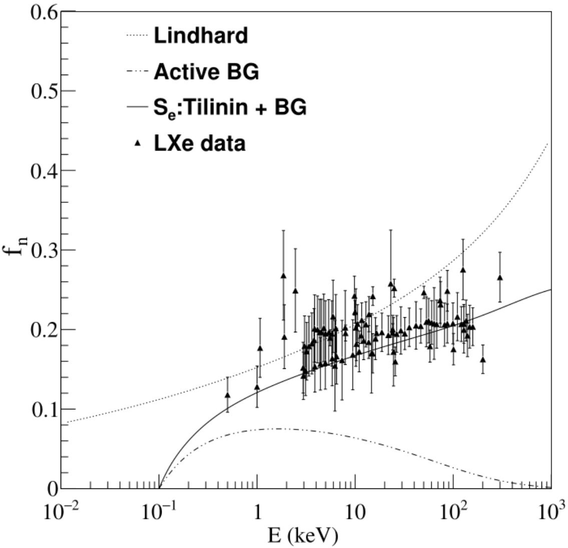
Lindhard
Active BG
S_e:Tilinin + BG
LXe data
f_n
0.6
0.5
0.4
0.3
0.2
0.1
0
10^{-2}
10^{-1}
1
10
10^2
10^3
E (keV)

Box size model
The box size is defined by electrostatic length scale (Dahl).

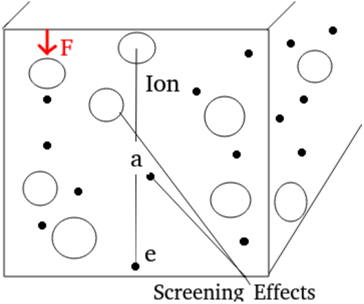

The box size is about $\approx \mu$m.

- The box size is much larger than the inter-atomic distance,
- Screening effects are considerable.
- We use Lindhard-Thomas-Fermi model $\varepsilon(k,0) = \varepsilon^0_{LAr}(1 + \frac{\kappa^2}{k^2})$.
- This modify the potential is

$$\phi^e_{ZS}(x_a, \xi_e, N) = \phi^e_Z(x_a, \xi_e, N) e^{-\kappa x a \xi_e^{2/3}}$$

- κ depends of the range $2r_{atom}$ to $2r_W$.
- $\Delta x_{\mathrm{LAr}}/\Delta x_{\mathrm{LXe}} = 1{,}6$
- The box size can be obtained from, $\phi^e_{ZS}(x_a, \xi_e, N) = \xi_e^{2/3} e a x_a F$.

We get a power law for the TIB parameter ξ.

$$a_{box} = \frac{(9{,}5\ \mathrm{nm})}{F^{\eta_0}}\left(\frac{V}{cm}\right)^{-\eta_0}, \quad \xi_{LAr} = \frac{\alpha N_i}{4a_{box}^2 F} = \frac{(0{,}37 \pm 0{,}07)N_i}{F^{(1-2\eta_0)}}\left(\frac{V}{cm}\right)^{2\eta_0 - 1}.$$

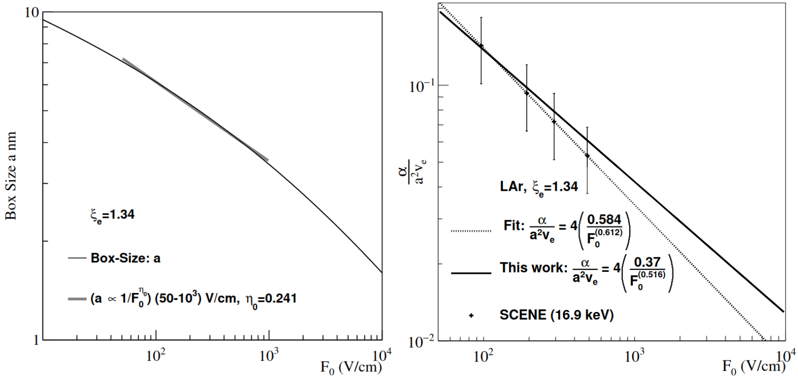

From LAr fit, we get the TIB parameter for LXe.

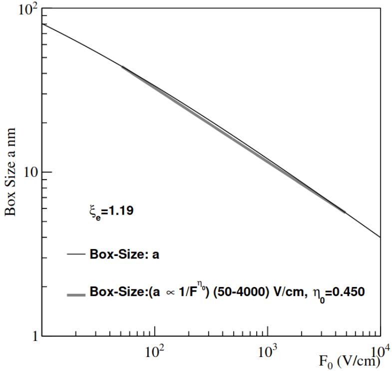

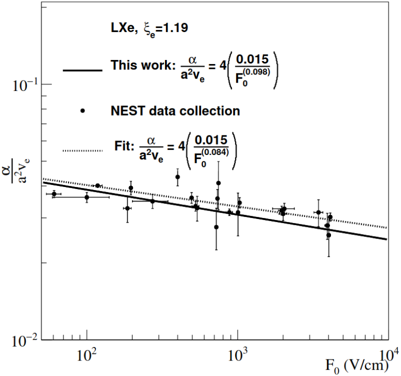

Electric Field Effect

Stark Effect for ions inside the Box

- Electric field F applied to a TPC.
- During recombination we have plasma formed by ions-electrons.
- The polarizability increase significantly $\varepsilon(k) \gg \varepsilon$
- We can compute the energy correction δ_1 to the potential $e\phi_Z(x, \xi_e) =< \psi \mid V \mid \psi >$,

$$\delta_1 =< \psi \mid V_{ext} \mid \psi >, \; V_{ext} = \pm((\xi_e)^{2/3} a x_z eF) = \pm((\xi_e)^{2/3} axeF) cos(\theta).$$

- Where $V_{ext} \ll \phi_Z(x, \xi_e)$ and $r \approx r_0 + dcos(\theta)$.
- We define the new electron-atom disturbed potential, $\phi_Z^e(x, \xi_e, Z, F) = \phi_Z^e(x, \xi_e, Z, 0) - \delta_1$.

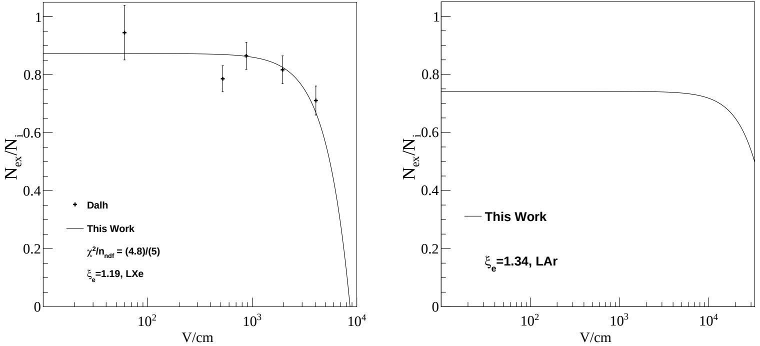

Figura: N_{ex}/N_i for LXe and LAr as function of the electric field.
In LAr predict a breakdown voltage of 60 $\mathrm{kV/cm}$ compared to experimental results $\approx$ 40 $\mathrm{kV/cm}$ (LIDINE-2025)

Skipper CCD

Overview

- **Skipper CCDs** (Skipper Charge-Coupled Devices) are ultra-low-noise imaging sensors capable of **sub-electron readout precision**.
- A CCD pixel accumulates charge from incident photons or particles.
- The Skipper architecture allows *N* **multiple non-destructive reads**.
- Each read adds independent noise, which can be statistically reduced:

$$\sigma_N = \frac{\sigma_1}{\sqrt{N}}$$

- Developed for **rare-event searches**,
- For applications in:
  - Dark matter detection (SENSEI, DAMIC-M) and CEνNS.
  - X-ray spectroscopy and low-light imaging.

Experiments

SENSEI, DAMIC-M, Oscura, CONNIE, MINER, and others exploit the Skipper CCD's ultra-low noise to explore new physics at low energies.

Instituto de Ciencias Nucleares UNAM

Skipper CCD Architecture

- Consists of:
  - **Buried channel CCD array**
  - **Floating gate amplifier** allowing non-destructive charge measurement
  - **Output stage** with correlated double sampling (CDS)
- Dynamic range: up to 10^4 electrons per pixel.
- Dark current: $\sim 10^{-3}$ e^-/pix/hour (at 140 K).
- Capable of achieving **noise below 0.1 e^- RMS**.

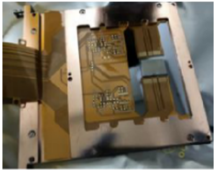

Skipper CCD: 1022×682 pix
$15 \times 15 \mu m^2$, $675 \mu m$ thick,
0.5 g total mass.

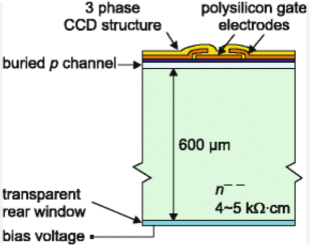

- At ICN detector Lab., we have a Kurt Lesker high vacuum capsule (3).
- Couple to a cold finger PT-90 (3-a) and a vacuum pomp Hi-cube Pfeiffer .
- Piezoelectric pressure sensor (3-b).
- Temperature control system (2).

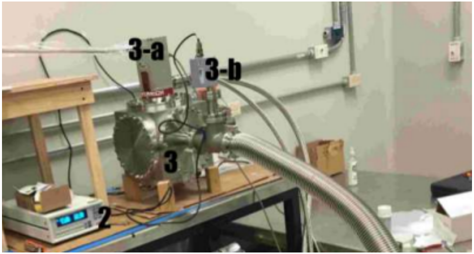

- Pressure lower than 10^{-5} Torr is reach inside the capsule.
- Temperatures up to 100 K.
- Electrostatic protection.

^{55}Fe X ray source

- We put a ^{55}Fe X ray source at 5 cm of the CCD.
- The source up to now have 0.13 μ Ci.
- We expect 15 photons per second at the CCD.

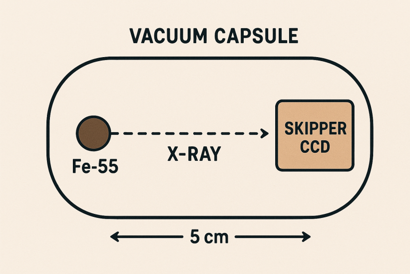

- The temperature of the sensor was set to 130 K.
- Exposure time of $\approx 3hrs$ per image.
- We take images with 300 samples continuously.

^{55}Fe X ray source

- I developed an algorithm to read clusters of pixels (3×3) produced by photons.
- We read the over-scan region, and fit with two Gaussian's.
- If the fit success, we save the image.
- Then over-scan region is subtracted.

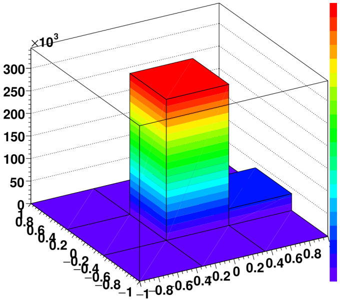

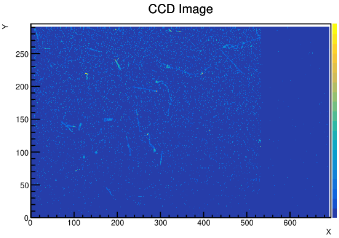

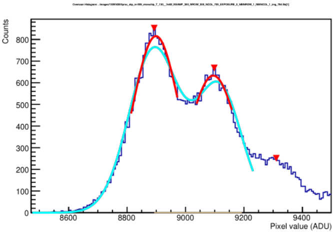

Main Peaks

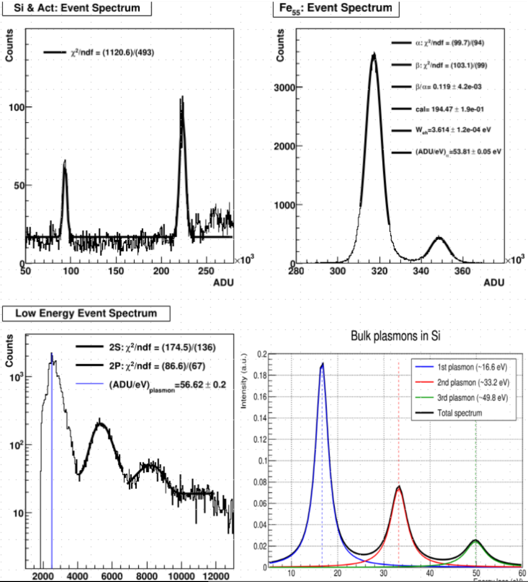

Main K_α and K_β identified

Escape K_α and Si peaks appear

Low energy forms, 2*s*, 2*p*

and plasmon peaks.

From Lindhard dielectric function

we have resonant plasmons peaks

in Si: 16.6 eV, 33.2 eV **49.8 eV**

Intensity $\propto Im\left(\frac{1}{\varepsilon(k,\omega)}\right)$

Systematics and Calibration

- For the selected images we have **fluctuations in over-scan value.**
- This error propagate in the data.
- We can estimate a systematic error: $\sigma^2 \propto \delta E^2$ ($\delta \approx 3 \times 10^{-3}$).

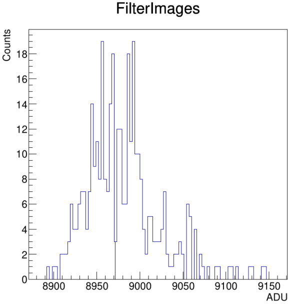

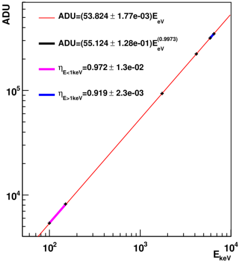

- Other systematic comes from **finite charge collection**[8]**.**
- Probability of observing $n - k$ charges given initial n charges.
- Binomial distribution: $< n >= n_M = \eta n$ and $\sigma_B^2 = \eta n(1 - \eta)$.

[8] PRD 102, 063026 (2020)

Calibrated Peaks

- Precision peaks calibrated.

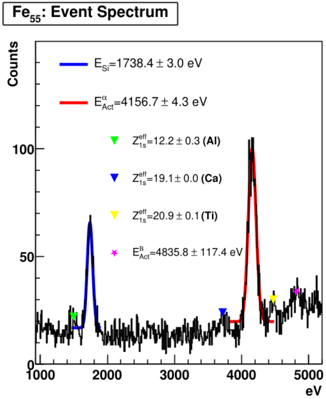

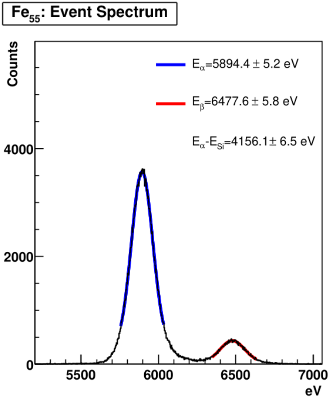

- We can identify impurities inside the capsule.

Low Energy Calibrated Peaks

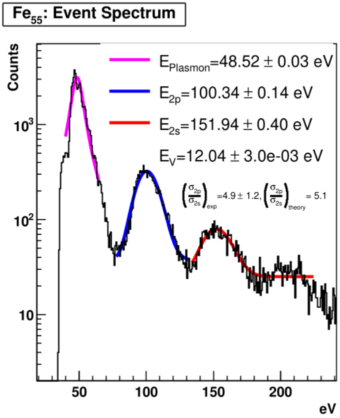

- We use the plasmon peak to obtain the valence band width.

$$\omega^2 = \frac{e^2 N_e}{m_e \varepsilon_0}, \quad E_v = \frac{\hbar^2}{2m_e}\left(3\pi^2 N_e\right)^{2/3}.$$

- We measure the average binding energies of the 2*s* and 2*p* electronic orbitals.
- Photoelectrons produced by the main $^{55}\mathrm{Fe}$ peaks activate this low energy peaks (mostly).
- We can measured the ratios amplitude of the 2*p* and 2*s* peaks.
- We check that compare to the ratio of e-Atom cross sections.

Electronic Fano Factor Measurement

- Using $\sigma^2 = \sigma_0^2 + \mathrm{F_e WE} + \sigma_\mathrm{B}^2 + \delta\mathrm{E}^2$, we measure the Fano factor ($\sigma_0 \approx 6$ eV).
- Main points are the K_α and K_β from $^{55}\mathrm{Fe}$.

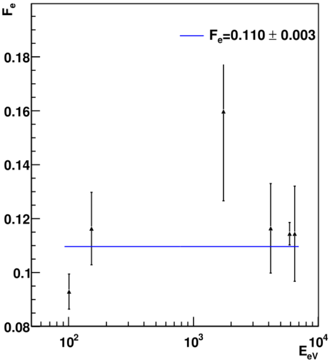

- Silicon peak shared escape peak events.
- 2*p* and 2*s* peaks have plasmon noise.

Second Analysis

- Previous plots show possible extra systematics.
- Plasmon peaks, Auger electrons and contamination peaks.
- We can use Voigt profile,

$$V(E;\sigma,\gamma) \equiv \int_{-\infty}^{\infty} G\left(E';\sigma\right) L\left(E-E';\gamma\right) dE', \quad G(E;\sigma) \equiv \frac{e^{-\frac{E^2}{2\sigma^2}}}{\sqrt{2\pi}\sigma}, \quad L(E;\gamma) \equiv \frac{\gamma}{\pi\left(\gamma^2+E^2\right)}$$

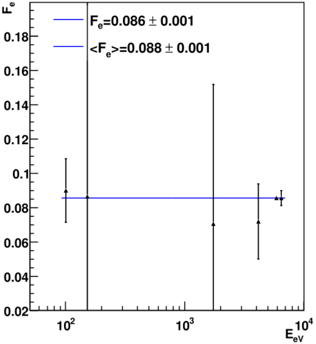

- We search for γ such that minimizes χ^2.

Complementary Analysis

- We can have Friedel oscillations in Si.
- When an electron is remove from the Fermi level.

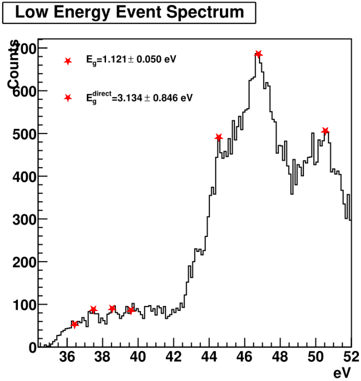

- This produces an oscillatory potential $\phi \propto cos(2k_F r)/r^3$.
- Can induce inter band transitions ($E_g^{Indirect} = 1{,}16$ eV and $E_g^{Direct} = 3{,}2$ eV).

Experiment to determined Nuclear Ionization Efficiency

- Use α particle source to produced silicon recoils in in the CCD.
- With Au foils (2μ), between the source and the sensor, to reduce α particle energy.

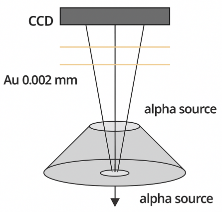

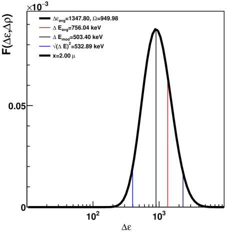

- We can measure the α deposition energy distribution.
- We can use the previous calibration for energy reconstruction.

Au Foils experiment at ICN Det. Lab

- Both α and Si recoils can be modeled by the integro-differential equation.
- We can estimate the energy fraction that goes to Si,

$$-\frac{1}{2}\varepsilon S_e^{\alpha}(\varepsilon)\left(1+\frac{W^{\alpha}(\varepsilon)}{S_e^{\alpha}(\varepsilon)\varepsilon}\right)\bar{\nu_{\alpha}}''(\varepsilon)+S_e^{\alpha}(\varepsilon)\bar{\nu_{\alpha}}'(\varepsilon)=\int_{\varepsilon u}^{\varepsilon^2}dt\,\frac{f\left(t^{1/2}\right)}{2t^{3/2}}\left[\bar{\nu_{\alpha}}(\varepsilon-t/\varepsilon)+\bar{\nu_{Si}}(t/\varepsilon-u)-\bar{\nu_{\alpha}}(\varepsilon)\right], \tag{5}$$

- S^{α} and W^{α} are very well know.
- $\varepsilon_{\alpha}=\bar{\nu}_{\alpha}(\varepsilon_{\alpha})+\bar{\eta}_{\alpha}(\varepsilon_{\alpha})$
- and $\bar{\nu}_{\alpha}(\varepsilon_{\alpha})=\bar{\nu}_{Si}(\bar{\nu}_{\alpha}(\varepsilon_{\alpha})-u)+\bar{\eta}_{Si}(\bar{\nu}_{\alpha}(\varepsilon_{\alpha})-u)$.
- We can compute $f_n^{Si}=\frac{\bar{\eta}_{Si}(\bar{\nu}_{\alpha}(\varepsilon_{\alpha})-u)}{\bar{\nu}_{\alpha}(\varepsilon_{\alpha})}$ and we can measure $f_n^{*}=\frac{\bar{\eta}_{Si}+\bar{\eta}_{\alpha}}{\varepsilon_{\alpha}}$.
- A raw analysis show that we can measure f_n^{Si}in the energy range $5-30$ keV.

Conclusions

Conclusions

- We have develop a formal theory for nuclear ionization efficiency in pure crystals and noble liquids.
- It can be added physical phenomena that was absent in Lidnhard formula.
- We can also give kinematic criteria to validate data, useful for phenomenological studies..
- Demonstration of full operational Skipper-CCD at ICN detector laboratory.
- Measurement of the silicon valence band width, 2*p*, 2*s* and K_α energies.
- Experimental determination of the electronic Fano factor in silicon.
- We have the experimental setup ready to measure ionization efficiency in silicon with α particles.
- This work has been presented in national and international workshops e.g.: RADPyC,TAUP, Magnificent CEνNS, EXCESS and LIDINE.

Instituto de Ciencias Nucleares UNAM

Acknowledgements

SECIHTI programa "Postdocs por México"
SECIHTI grant CF-2023-I-1169, y por los proyectos
DGAPA-UNAM PAPIIT-IN106322, PAPIIT-IT100420 y SNII.

Backup

Effective Field Theory and Lagrangians

SM effective Lagrangian:

$$\mathcal{L}_{\text{SM}} = -\frac{G_F}{\sqrt{2}} \sum_{q=u,d} \left[\bar{\nu}\gamma_\mu(1-\gamma_5)\nu \; \bar{q}\gamma^\mu(g_V^q - g_A^q\gamma_5)q \right]$$

- $g_V^u = \frac{1}{2} - \frac{4}{3}\sin^2\theta_W$, $g_V^d = -\frac{1}{2} + \frac{2}{3}\sin^2\theta_W$
- $g_A^u = \frac{1}{2}$, $g_A^d = -\frac{1}{2}$

BSM extension (dimension-5–7 operators):

$$\mathcal{L}_{\text{BSM}} = \sum_q \left[C_V^q \, \bar{\nu}\gamma_\mu P_L \nu \, \bar{q}\gamma^\mu q + C_A^q \, \bar{\nu}\gamma_\mu P_L \nu \, \bar{q}\gamma^\mu\gamma_5 q + C_S^q \, \bar{\nu} P_L \nu \, m_q \bar{q} q + C_T^q \, \bar{\nu}\sigma_{\mu\nu} P_L \nu \, \bar{q}\sigma^{\mu\nu} q \right]$$

- Allows for vector, axial, scalar, tensor, and dipole interactions beyond the SM.

CEνNS and DM Motivations

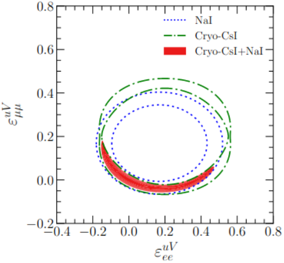

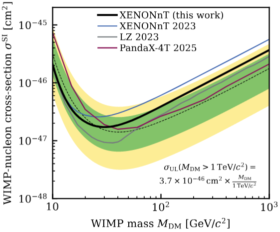

Figura: 90 % C.L for NSI, (PRD 110, 095027) and recent XenT DM limit (arXiv:2502.18005v1)

J.HEP 2022 127 (2022)

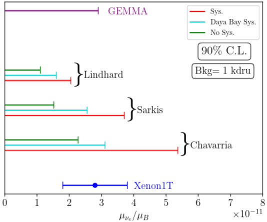

μ_B constraints & yields for solar ν studies

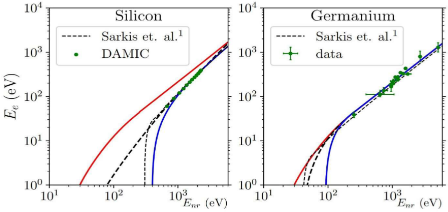

PRD 106 015002 (2022)

Instituto de Ciencias Nucleares UNAM

Results

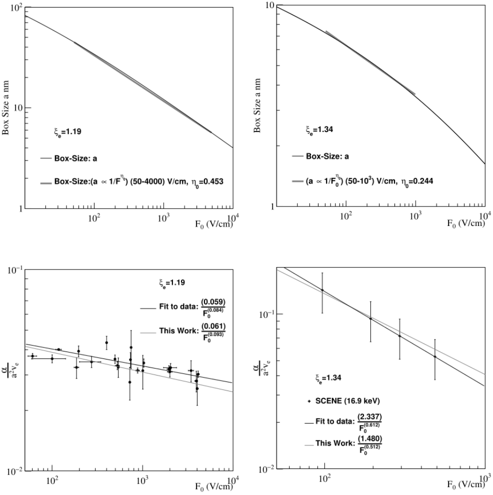

- Using the screen atom potential for ions,

$$-e\phi_Z^e(x', \xi_e, N) = \frac{Ze^2}{bx'}\left[\left(\frac{N}{Z}\right)(\chi_Z(x') - 1) + 1\right].$$

- We can use Dahl electrostatic interpretation for Box size determination,

$$-bzF = (\phi_Z^e(z, \xi_e, N))_{\mathrm{sc}},$$

- Box size, depends weakly of electric field for high Z.
- With these model, we can estimate the recombination parameters.
- For LNe, LAr, LKr and LXe we have **16 parameters reduced to 1!**

Multi-Chip-Module (MCM) offers a compact arrangement of sensors:

- 16 Skipper-CCD sensors on the same module, 32x increase in mass (8 g).
- Designed for the Oscura experiment.
- Multiplexed readout.
- A MCM was installed at CONNIE in May 2024:
- New vacuum interface and multiplexer boards.

Multi-Chip Module
(16 CCDs → 8 g)

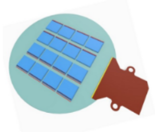

Super Module
(16 MCMs → 100 g)

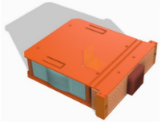

Oscura design [JINST 18 (08), P08016]

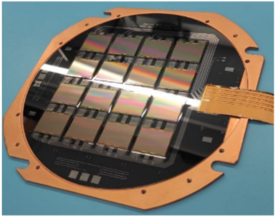

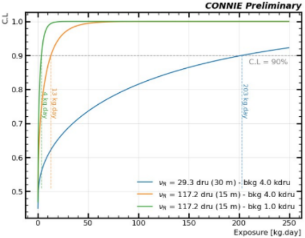

CEνNS search in the lowest-energy bins of reactor ON − OFF rates.

- Updated neutrino flux model with improved antineutrino spectra for ^{235}U,^{238}U, ^{239}Pu and ^{241}Pu.
- Updated Sarkis quenching factor model for Si. (*PRA 107, 062811 (2023)*)
- Improved descriptions of the electronic stopping, interatomic potential and electronic binding at sub-keV energies, $E_{nr} > 0.24$ keV$_{nr}$ (15 eV$_{ee}$).

Measured Energy [keV$_{ee}$]	Sarkis (2023) rate [kg^{-1}d^{-1}keV$_{ee}^{-1}$]	Chavarria rate [kg^{-1}d^{-1}keV$_{ee}^{-1}$]	Observed 95% C.L. [kg^{-1}d^{-1}keV$_{ee}^{-1}$]	Expected 95% C.L. [kg^{-1}d^{-1}keV$_{ee}^{-1}$]
0.015 – 0.215	$29.3^{+4.6}_{-4.7}$	17.7 ± 3.3	2.24×10^3	3.18×10^3
0.215 – 0.415	$2.7^{+1.3}_{-1.2}$	2.20 ± 0.21	7.36×10^3	4.77×10^3
0.415 – 0.615	$0.43^{+0.41}_{-0.39}$	0.36 ± 0.04	3.41×10^3	3.31×10^3

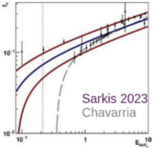

arXiv:2403.15976

- Observed limit at 76x the expected SM predicted Rate (with Sarkis QF).
- Comparable to our previous limit with standard CCDs and 10^3 larger exposure.

- Below ~ 1 keV$_{nr}$, uncertainties dominate.
- Over-reliance on Lindhard fits may obscure real deviations.
- Calibration conditions often differ from physics runs.
- “Anchored to Lindhard” data.

Mean "Anchored to Lindhard"

- E_r is infer from neutron scattering or simulation.
- Analysis often assumes Lindhard functional form when converting measured signals.
- When the energy calibration or background subtraction depends on assumptions about how QF.
- Analysis is no longer fully model-independent.
- At low energies ($E_r < 1$ keV), small systematic shifts in QF have large effects.
- Real understanding requires model-independent analysis.
- Thus, data are **"anchored" to a model shape** rather than fully empirical.
- Model anchoring can produce an **illusion of agreement** with theory.

Instituto de Ciencias Nucleares UNAM

Nuclear Stopping Power

Collision between two atoms, and can be described by classical kinematics.

The projectile in the medium can hit a target ion transferring some of its energy.

Using the atom-atom inter-atomic potential we compute the nuclear cross section σ_n.

These define the nuclear stopping power $S_n = \int \sum T_n d\sigma_n$.

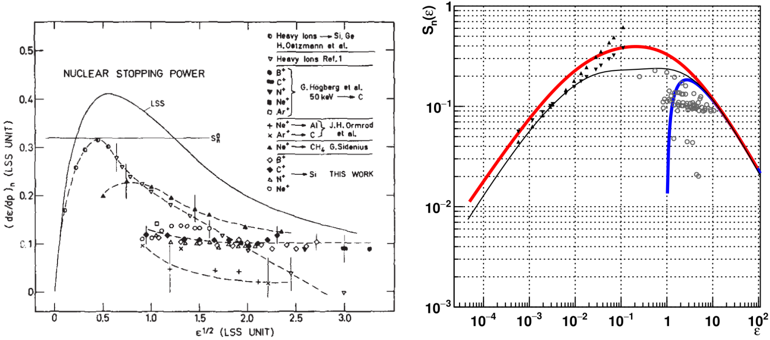

Figura: (left) LSS Nuclear Stopping and data, (right) Optical model approach (future publication).